Intelligent Systems with Applications 16 (2022) 200124

Contents lists available at ScienceDirect

Intelligent Systems with Applications

journal homepage: www.journals.elsevier.com/intelligent-systems-with-applications

Online estimation of unknown aerodynamic forces acting on AWE systems

Nacim Meslem *, Jonathan Dumon, Ahmad Hably, Asmae El Ayachi, Audrey Schanen

CNRS, Grenoble INP, GIPSA-Lab, Université Grenoble Alpes, Grenoble 38000, France*

ARTICLE INFO

Keywords:
AWE systems
Aerodynamic forces
Nonlinear systems
State and input estimation
Extended Kalman filter

ABSTRACT

Airborne Wind Energy systems (AWE) represent a promising solution to environmental challenges that has revolutionized research in the wind industry. The studied AWE system in this work is equipped with a multi-copter drone in order to perform take-off and landing maneuvers and the objective consists in presenting an estimation strategy based on an Extended Kalman Filter (EKF) to obtain accurate estimation of the aerodynamic forces needed to improve the performance of the proposed control law for the considered prototype in this study. The proposed method is implemented and tested in a numerical and experimental environment. The obtained results show the effectiveness of the introduced method at estimating unknown forces that act on the system despite the presence of several sources of uncertainty: neglected nonlinearities, poorly known parameters, physical constraints, etc. Moreover, we show that the knowledge of these forces allows one to improve the robustness of the studied AWE system during its take-off and landing phases.

1. Introduction

Airborne Wind Energy (AWE) systems aim at harvesting high altitude wind energy (Archer & Caldeira, 2009; Canale et al., 2010). AWE systems are divided into two classes depending on the place where energy is produced (Ahrens et al., 2013; Schmehl, 2018). First the on-board production systems where classical wind turbines are lifted to high altitudes and electric energy is produced in the sky and transmitted to the ground through conductive tethers. The second solution is the on-ground production systems where the device follows a predefined trajectory and generates aerodynamic lift and drag forces that are transferred via the tether to the on-ground station to be converted into electrical power. On the other hand, on-ground systems have two phases: The traction phase, where aerodynamic forces are transmitted by tethers to turn an on-ground machine and the recovery phase, where the wing is reeled-in, an operation that consumes energy.

The delivered research results are gradually assessing and eliminating feasibility risks. The numerous advantages of these energy systems can be lower installation costs, high energy capacity factors, higher flexibility (see Ahmed et al. (2012) for a survey on soft kites and Cherubini et al. (2015) for AWE systems in general). Currently, in the research community, there are many innovative designs regarding the airborne platform. The choice of the platform depends on the lifting capabilities of the aerodynamic surface. Classically, kites and unmanned aerial vehicles (UAV) have been used as the airborne platform. But many other innovative concepts are being explored such as Magnus cylinders (Hably et al., 2018a), rotary kites, balloons etc.

The knowledge of the aerodynamic behavior of the airfoil is crucial for several control strategies proposed in the literature (Schanen et al., 2021; Zgraggen et al., 2014). It is of great interest to estimate accurately the unknown forces that act on the wing. In Williams et al. (2008), a nonlinear feedback controller is used to stabilize the system motion using a set of noisy measurements. An on-line estimation of system parameters describing the kite state is studied in Millane et al. (2015). The estimation scheme fuses measurements from range sensing, based on ultra-wideband radios, and inertial readings from an inertial measurement unit. In Schmidt et al. (2017), employing only ground-based measurements, an Extended Kalman Filter Daum (2015); Ljung (1979); Simon (2010) is used to estimate the airfoil position, velocity and acceleration. A similar approach has been studied in Hjukse (2011). An unscented Kalman filter algorithm is tested in simulation environment in Ranneberg (2013) with different sensor setups including airborne sensors (acceleration, airspeed pressure, GPS velocity and position measurements) and on-ground-based measurements. In this present work, an EKF is proposed to reconstruct online the whole state vector of the system, as well as the sum of the unknown forces that act on it such as the aerodynamic forces (lift and drag), dry frictions, propeller performance variations, etc. This allows one: (*i*) to improve the control performance of the nonlinear controller proposed in Schanen et al. (2021) by including the estimated unknown forces in the control design

* Corresponding author.
E-mail address: nacim.meslem@grenoble-inp.fr (N. Meslem).

https://doi.org/10.1016/j.iswa.2022.200124
Received 18 December 2021; Received in revised form 25 June 2022; Accepted 3 September 2022
Available online 11 September 2022

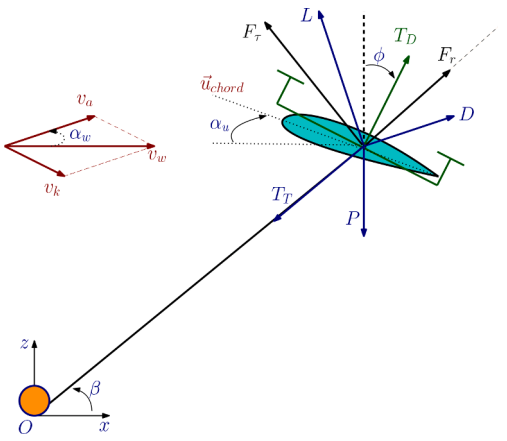

Fig. 1. The forces acting on the airborne wind energy system with the drone connected to the on-ground station.

step. (*ii*) to estimate the aerodynamic coefficients that are of great interest in order to evaluate the aerodynamic performance of the AWE system.

The paper is structured as follows. The model of the studied system is presented in Section 2. The objectives of this work are detailed in Section 3. In Section 4, the EKF theory used in the paper is presented. Finally, simulation and experimental results using EKF are discussed in Section 5. The paper ends by a conclusion.

2. Mathematical modeling

In this present paper, the airborne wind energy (AWE) system under study is composed of two parts: The first one is composed of a rigid wing attached to a multicopter and the second part is an on-ground station. Both parts are connected by means of a tether. In presence of wind, the flying device generates aerodynamic lift and drag forces. The resultant traction force is transmitted via the tether to the on-ground station to convert the tether's linear motion into a shaft power that drives a generator. The thrust force generated by the multicopter is used to control the trajectory of the system especially in absence of wind.

The different forces acting on the system are represented in Fig. 1: The aerodynamic forces, L and D, the weight P, the tether tension T_T and the thrust of the drone T_D. The drag force D is aligned in the direction of apparent wind v_a whereas the lift force L is orthogonal to it. The apparent wind velocity $\vec{v}_a$ is given by:

$$\vec{v}_a = \vec{v}_w - \vec{v}_k \tag{1}$$

where $\vec{v}_k$ is the translation velocity of the flying device and $\vec{v}_w$ is the wind speed. The angle of attack (AoA) is defined as the angle between the apparent wind velocity $\vec{v}_a$ and the chord line $\vec{u}_{chord}$:

$$AoA = \angle\left(\vec{v}_a, \vec{u}_{chord}\right) \tag{2}$$

The pitch angle α_u is determined with respect to the horizon and chord line $\vec{u}_{chord}$:

$$\alpha_u = \angle\left(\vec{x}, \vec{u}_{chord}\right) \tag{3}$$

Several wing configurations can be studied. Notice that, the absence of an actuator that links the drone to the wing, leads to a fixed relative angle, α_u can be expressed as:

$$\alpha_u = \phi + \alpha_D \tag{4}$$

where α_D is a fixed design value. In this present study, only the system motion in the vertical plane is considered, assuming that the system is aligned to the main wind direction and it only experiences small variations in the third dimension. It is also assumed that the tether of length r forms a straight line. Note that, this assumption is valid for tethers with small length, where drag and weight of the cable are negligible w.r.t tether tension, and tether elasticity is weak. The tether has an elevation angle β with respect to the horizontal plane. The drone has an inclination angle ϕ with respect to the vertical axis and produces a thrust force T_D. The combined mass of all airborne system components is denoted by M_M. Considering the system's two degrees of freedom, r and β, translation velocity of the flying device $\vec{v}_k$ can be decomposed into a radial velocity component $v_{k,r} = \dot{r}$ and a tangential velocity component $v_{k,\tau} = r\dot{\beta}$. As done in Hably et al. (2018b); Schanen et al. (2021), differentiation of $\vec{v}_k$ with respect to time yields a radial acceleration component and a tangential acceleration component:

$$\frac{dv_{k,r}}{dt} = \ddot{r} - r\dot{\beta}^2, \quad \frac{dv_{k,\tau}}{dt} = r\ddot{\beta} + 2\dot{r}\dot{\beta} \tag{5}$$

Table 1
System parameters.

Parameter	Definition	Value
M_M	Mass of airborne subsystem	0.774 kg
M_D	Ground station rotor mass	0.0481 kg
S	Wing area	0.09 m^2
ρ	Air density	1.225 kg/m^3

Based on the fundamental principle of dynamics, a 2D nonlinear model that describes the time evolution of the tether's length r and of the elevation angle β of this system can be then found:

$$\begin{cases} \ddot{r} = \dfrac{1}{M_M + M_D}\left(r\dot{\beta}^2 M_M - T_T - P\sin(\beta) + u_{T_0} + F_{a,r}\right) \\ \ddot{\beta} = \dfrac{1}{r}\left(-2\dot{\beta}\dot{r} + \dfrac{1}{M_M}\left(-P\cos(\beta) + u_\beta + F_{a,\tau}\right)\right) \end{cases} \tag{6}$$

where M_D is the ground station rotor mass and

$$\begin{cases} u_{T_0} = -T_D\sin(\beta + \phi) \\ u_\beta = T_D\sin(-\beta + \phi) \end{cases} \tag{7}$$

The tangential $F_{a,\tau}$ and radial $F_{a,r}$ forces in (6) could be viewed as compositions in between the aerodynamics forces ($F_{aero,r}$, $F_{aero,\tau}$) and other unknown forces ($F_{un,r}$, $F_{un,\tau}$) that could act on the system,

$$\begin{cases} F_{a,r} = F_{aero,r} + F_{un,r}, \\ F_{a,\tau} = F_{aero,\tau} + F_{un,\tau} \end{cases} \tag{8}$$

On the other hand, if the lift L and drag D forces are available, the aerodynamic forces can be computed as follows:

$$\begin{cases} F_{aero,r} = L\sin(\beta - \alpha_\omega) + D\cos(\beta - \alpha_\omega) \\ F_{aero,\tau} = L\cos(\beta - \alpha_\omega) - D\sin(\beta - \alpha_\omega) \end{cases} \tag{9}$$

Note that, in (9), α_ω stands for the angle formed by the apparent wind velocity with the horizontal, refer to Fig. 1.

$$\alpha_w = \angle\left(\vec{x}, \vec{v}_a\right) \tag{10}$$

This angle is calculated in Lozano et al. (2013) by the following formula,

$$\alpha_\omega = \arctan\frac{r\cos(\beta)\dot{\beta} + \dot{r}\sin(\beta)}{v_\omega + r\sin(\beta)\dot{\beta} - \dot{r}\cos(\beta)} \tag{11}$$

The involved parameters in model (6) are gathered in Table 1.

Now, from the coupled differential equations in (6), a state space representation of the AWE system depicted in Fig. 1 can be deduced by considering the following state vector:

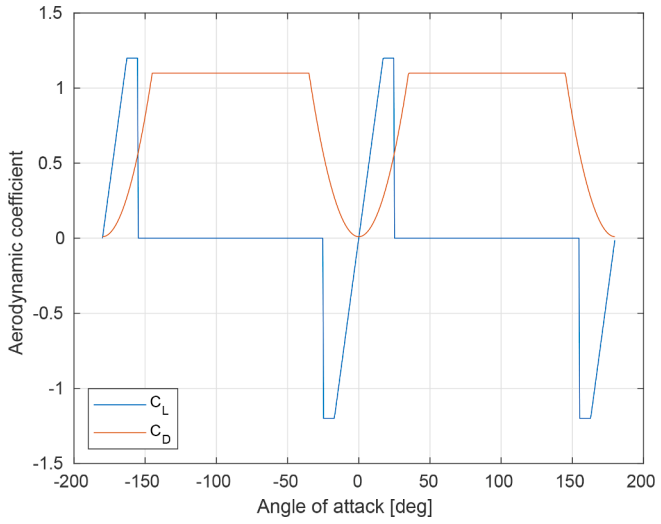

Fig. 2. Evolution of the aerodynamic coefficient C_L and C_D.

$$x = [x_1,\ x_2,\ x_3,\ x_4]^T = [r,\ \dot{r},\ \beta,\ \dot{\beta}]^T \tag{12}$$

This change of variables allows one to rewrite (6) as follows:

- State equation:

$$\dot{x} = \begin{pmatrix} x_2 \\ \frac{1}{M_M + M_D}\left(x_1 x_4^2 M_M - T_T - P\sin(x_3) + u_{T_0} + F_{a,r}\right) \\ x_4 \\ \frac{1}{x_1}\left(-2x_4 x_2 + \frac{1}{M_M}\left(-P\cos(x_3) + u_\beta + F_{a,\tau}\right)\right) \end{pmatrix} \tag{13}$$

- Output equation:

$$y = \begin{pmatrix} x_1 \\ x_3 \end{pmatrix} \tag{14}$$

2.1. System uncertainties

In practice, the lift and drag forces can be computed, if the apparent wind velocity is available, by the following formula:

$$\begin{cases} L = \frac{1}{2}\rho S v_a^2 C_L \\ D = \frac{1}{2}\rho S v_a^2 C_D \end{cases} \tag{15}$$

where ρ is the air density, v_a is the apparent wind velocity, S is the considered wing surface, C_L and C_D are respectively aerodynamic lift and drag coefficients. To obtain the numerical values of these coefficients, one can refer to the aerodynamic coefficient curves of Fig. 2, generated from the mathematical model presented in Eq. (16) which is borrowed from Lozano et al. (2013),

$$\begin{cases} C_L = 0.07(AoA) \\ C_D = \frac{1}{1.75\pi}C_L^2 + 0.1 \end{cases} \tag{16}$$

where the angle of attack can be computed by $AoA = \alpha_u - \alpha_\omega$ using formulas (4) and (11).

However, usually in real world applications, the wind velocity is an unknown variable or imprecisely measured. Thus, the radial and tangential forces defined in (9) and used in (8) are unknown or poorly known. This renders model (13) uncertain.

Moreover, as mentioned before, the AWE system is also affected by others unknown forces that can be added to the tangential and radial aerodynamic forces as shown in (8). For instance, one can consider the dry friction and the forces due to propeller performance variation. In this case, the radial and tangential unknown forces that could act on the system can be expressed as follows:

$$\begin{cases} F_{un,r} = F_{fric,r} + F_{prop,r}, \\ F_{un,\tau} = F_{prop,\tau} \end{cases} \tag{17}$$

This fact, increases highly the uncertainty in model (13) and impacts largely its accuracy. Thus, it is of great interest to be able to estimate these unknown forces in order to obtain a more precise model of the real system and to master farther its dynamical behavior.

Remark 1. In (17), $F_{fric,r}$ stands for the dry friction of the on-ground winch, while F_{prop} stand for the forces due to the embedded battery voltage variation as well as to the influence of airflow on propellers efficiency. In this study these forces are implemented as follows:

- $F_{fric,r}$ is represented by a classical static friction model using $F_k \text{sign}(\dot{r})$ to compute kinetic friction after a threshold of static friction F_s. We have chosen $F_s = 0.8$ N and $F_k = 0.5$ N.
- F_{prop} is considered as a modeling error on the drone's thrust and it is set to $0.05T_D$. Then, by projection into radial and tangential directions one gets $F_{prop,r}$ and $F_{prop,\tau}$.

3. Problem statement

As introduced in the above section, the AWE system presented in Fig. 1 is subjected to many poorly-known or completely unknown forces that affect its desired performance, namely the precision and the robustness of the tracking of a specified set-point. Thus, estimating these forces in presence of other sources of uncertainty, like measurement noise etc., is a challenging problem in automatic control field. Thus, the goal of this work consists in improving the performance of the nonlinear control strategy proposed in Schanen et al. (2021) for system (6) by considering several aspects:

- *Precision and robustness*: In Schanen et al. (2021) the unknown forces are considered as exogenous disturbances and integral actions are applied on the tracking error to guarantee the robustness of the proposed controller. Unfortunately, we observed that for large wind velocities, this control approach fails to fulfill the desired performance. Thus, to overcome this drawback, we propose in a first step an estimator for these forces. Then the estimated values will be used in the control design step in order to better master the nonlinearities of the system.
- *Insensitivity to measurement noise*: In Schanen et al. (2021), the state variables $\dot{r}$ and $\dot{\beta}$ used in the control law are estimated by numerical methods. Thus, the precision of these estimations depends mainly on the quality of the used sensors. It is worth pointing out that adding more sensors is not the ultimate solution for precise measurements. The cost and weight of additional sensors can also be a problem and source of more uncertainties. Thereby, to be insensitive to the measurement noises and without using additional sensors, we propose to apply an EKF to estimate these variables from the measurements of the length of the tether and the elevation angle.
- *Estimating the aerodynamic coefficients*: Based on (15), the estimation of aerodynamic forces acting on the system together with an accurate measurement of the wind velocity allows one to determine the aerodynamic parameters that characterize the behavior of the

considered AWE system. This knowledge is of great interest in order to evaluate the aerodynamic performance of the system and to establish reliable models of these coefficients.

Thus, to achieve the above mentioned objectives, based on the available output data (the tether's length and its elevation angle), an extended Kalman filter will be designed to estimate the whole state vector (12) of the system and the additional unknown forces (8). To do that, an augmented model of (13) is required. Notice that, in this augmented model the unknown forces (8) should be considered as state variables with zero dynamics. Thus, by the use of the following augmented state vector:

$$z = [z_1,\ z_2,\ z_3,\ z_4,\ z_5,\ z_6]^T = [r,\ \dot{r},\ \beta,\ \dot{\beta},\ F_{a,r},\ F_{a,\tau}]^T \tag{18}$$

the state space representation (13), can be transformed to the needed augmented model:

$$\dot{z} = \begin{pmatrix} z_2 \\ \frac{1}{M_M + M_D}\left[z_1 z_4^2 M_M - T_T - P\sin(z_3) + u_{T_0} + z_5\right] \\ z_4 \\ \frac{1}{z_1}\left[-2z_4 z_2 + \frac{1}{M_m}\left(-P\cos(z_3) + u_\beta + z_6\right)\right] \\ 0 \\ 0 \end{pmatrix} \tag{19}$$

where the two components of the observation vector are the tether length $r = z_1$ and the elevation angle $\beta = z_3$

$$y = \begin{pmatrix} z_1 \\ z_3 \end{pmatrix} \tag{20}$$

To sum up, based on the augmented model (19) and (20), the objective of the proposed extended Kalman filter is to estimate both the state vector of (13) and the unknown forces (8). This allows one : (*i*) to improve the control strategy introduced in Schanen et al. (2021) and (*ii*) to get accurate estimations of the aerodynamic coefficients C_L and C_D.

Remark 2. It is worth pointing out that, based on Eq. (15) the knowledge of the aerodynamic forces (Drag D and Lift L) and the aerodynamic coefficients (C_L and C_D) allows one to get an estimation of the apparent wind velocity v_a.

4. Extended Kalman filter (EKF)

Extended Kalman filter is an algorithm able to estimate the state vector of a nonlinear system from incomplete or noisy measurements of its outputs allied with a discrete-time-varying linearized model that describes its dynamics. In this work, to design the needed discrete-time linearized model, we have first to linearize (19) around the current state vector and then to discretize the obtained linear equations. For the sake of simplicity, let us represent the augmented system (19)-(20) by

$$\begin{aligned} \dot{z} &= f(z,u) \\ y &= Hz \end{aligned} \tag{21}$$

where $u = (T_T, u_{T_0}, u_\beta)^T$ and we denote by H the following output matrix

$$H = \begin{bmatrix} 1 & 0 & 0 & 0 & 0 & 0 \\ 0 & 0 & 1 & 0 & 0 & 0 \end{bmatrix} \tag{22}$$

Thus, the first order linearization of (21) around its the current state vector z_k leads to the following approximation:

$$\dot{z} \approx f(z_k, u_k) + A_k(z - z_k) + B_k(u - u_k) \tag{23}$$

where

$$A_k = \frac{\partial f(z,u)}{\partial z}\Big|_{(z_k,u_k)} \text{ and } B_k = \frac{\partial f(z,u)}{\partial u}\Big|_{(z_k,u_k)} \tag{24}$$

Now, to obtain the classical Kalman equations, we need to discretize (23). For this, we apply to (23) the Euler explicit discretization method, which allows one to get the following discrete model:

$$\begin{aligned} z_{k+1} &= F_k z_k + s_k \\ y_k &= Hz_k \end{aligned} \tag{25}$$

where $F_k = I_6 + hA_k$, $s_k = h(f(z_k,u_k) - A_k z_k)$, h stands for the considered discretization step and I_6 is an identity matrix of dimension 6. Hereafter, all the steps to implement the extended Kalman filter are listed.

- **Propagation stage**
  - Predicted state estimate:

    $$\widehat{z}_{k|k-1} = \widehat{z}_{k-1|k-1} + hf\left(\widehat{z}_{k-1|k-1}, u_{k-1}\right)$$

  - Predicted error covariance:

    $$P_{k|k-1} = F_k P_{k-1|k-1} F_k^T + Q$$

- **Correction stage**
  - Innovation:

    $$\widetilde{y}_k = y_k - H\widehat{z}_{k|k-1}$$

  - Residual covariance:

    $$S_k = HP_{k|k-1}H^T + R$$

  - Kalman gain:

    $$K_k = P_{k|k-1}H^T S_k^{-1}$$

  - Updated state estimate:

    $$\widehat{z}_{k|k} = \widehat{z}_{k|k-1} + K_k\widetilde{y}_k$$

  - Updated error covariance:

    $$P_{k|k} = (I_6 - K_k H)P_{k|k-1}$$

Although the covariance matrices Q and R are supposed to reflect the statistics of the measurement noises and state disturbances, in this work these matrices are used as tuning parameters that can be adjusted to get the desired performance.

The next section is devoted to show the performance of the proposed extended Kalman filter. First, in a simulation environment, this EKF is applied to estimate the state vector and the assumed unknown aerodynamic forces of system (13) governed by the control law introduced in Schanen et al. (2021). Then, we show that the robustness of this control law can be enhanced if the estimated forces are included when designing it. Finally, from experimental data, the aerodynamic forces and coefficients are reconstructed and compared to the results of the theoretical model.

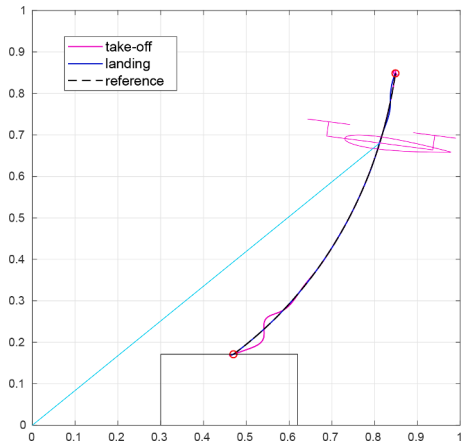

Fig. 3. Simulated trajectory and reference path of the AWE system for a wind speed of $v_w = 0$ m/s.

5. Simulation and experimental results

5.1. The considered control strategy

In Schanen et al. (2021) a state feedback nonlinear controller has been designed to steer the take-off and landing phases of the AWE system illustrated in Fig. 1. The flying part of this system has to follow up a user-defined trajectory as shown in Fig. 3. In this figure, the presented Cartesian coordinate hyperplane is YZ-plane, the green dotted line illustrates the tether and the bottom box represents the takeoff and landing platform.

The considered takeoff/landing scenario is described as follows:

1. Initial position: The system starts from its initial position at $r_0 = 0.4$ m, $\beta_0 = 20^\circ$, $T_{D_0} = 0$ N, and $\phi_0 = 0^\circ$.
2. Takeoff phase: At $t = 0$ s the reference signal r_d goes from r_0 to $r_f = 1.2$ m with a ramp rate of 0.08 m/s, and the desired elevation angle β_d goes from β_0 to $\beta_f = 45^\circ$ with a ramp rate of 0.5° /s.
3. Landing phase: At $t = 25$ s, the reference signal r_d goes from r_f to r_0 with a ramp rate of 0.08 m/s, and the desired elevation angle β_d goes from β_f to β_0 with a ramp rate of 0.5°/s.
4. End of the scenario: Once the system is landed, the drone is back to its initial position and ready to start a new cycle.

It is worth pointing out that the straight green dotted line in Fig. 3 represents the tether that links the drone to the on-ground station.

To accomplish this objective, flatness control theory is applied to design a control law able to deal with a part of the system nonlinearities and to ensure the stability of the tracking error (Fliess et al., 1995). On the other hand, integral actions (Jaulin (2015), Section 2.1.2, page 47) are added in the closed loop in order to cope with the neglected unknown forces that can affect the desired behavior of this system. The proposed controller in Schanen et al. (2021) has the following structure:

$$u = \begin{pmatrix} T_T \\ u_\beta \end{pmatrix} = A^{-1}(x)\Big(v - B(x)\Big) \tag{26}$$

where

$$A(x) = \begin{pmatrix} -\dfrac{1}{M_M + M_D} & 0 \\ 0 & \dfrac{1}{M_M x_1} \end{pmatrix} \tag{27}$$

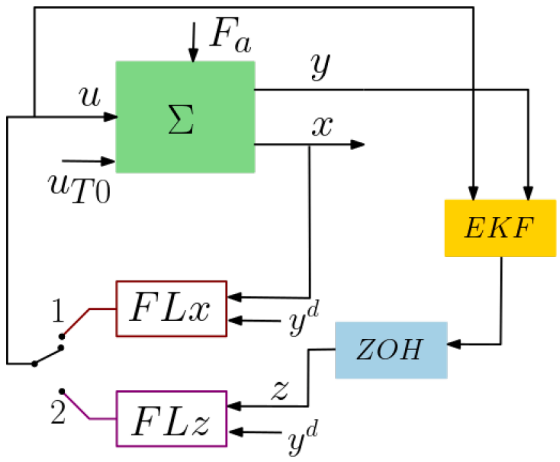

Fig. 4. Measured and estimated nonlinear state feedback control laws. Position 1 of the switch corresponds to the measured state feedback loop, while its Position 2 stands for the estimated state feedback loop.

$$B(x) = \begin{pmatrix} \dfrac{1}{M_M + M_D}\Big[x_1 x_4^2 M_M - P\sin(x_3) + u_{T_0}\Big] \\ \dfrac{1}{x_1}\Big[-2x_4 x_2 - \dfrac{P}{M_M}\cos(x_3)\Big] \end{pmatrix} \tag{28}$$

Interested reader can find in Schanen et al. (2021) the definition and the expression of v, as well as other control implementation details. The simplified block diagram of the proposed control strategy is presented by the first closed loop in Fig. 4, where the block Σ represents the system and the block *FLx* stands for the applied feedback linearization controller based on the measured state vector x.

As shown in Schanen et al. (2021), for low wind velocities, the proposed control method provides good tracking performance. However, for large wind velocities, the neglected aerodynamic forces (considered as disturbances) become important and the use of integral actions will no longer suffice to ensure the robustness of the system. Thus, estimating these unknown forces and integrating them in the control design is an issue of great interest. In this case, the new feedback linearization control law is designed as follows:

$$u = \begin{pmatrix} T_T \\ u_\beta \end{pmatrix} = A^{-1}(z)\Big(v - B(z)\Big) \tag{29}$$

where

$$A(z) = \begin{pmatrix} -\dfrac{1}{M_M + M_D} & 0 \\ 0 & \dfrac{1}{M_M z_1} \end{pmatrix} \tag{30}$$

$$B(z) = \begin{pmatrix} \dfrac{1}{M_M + M_D}\Big[z_1 z_4^2 M_M - P\sin(z_3) + u_{T_0} + z_5\Big] \\ \dfrac{1}{x_1}\Big[-2z_4 z_2 - \dfrac{P}{M_M}\cos(z_3) + z_6\Big] \end{pmatrix} \tag{31}$$

Note that, position 2 of the switch in Fig. 4 corresponds to the second closed loop, where in the block *LFz* the feedback linearization controller is applied based on the augmented estimated state vector z provided by the extended Kalman filter.

In what follows, the extended Kalman filter introduced in Section 4 is tested and validated in a simulation environment. More precisely, for the different experiments presented in the next Section, the EKF is not integrated in the control loop but used only to reconstruct online the state vector of the system and to estimate the assumed unknown

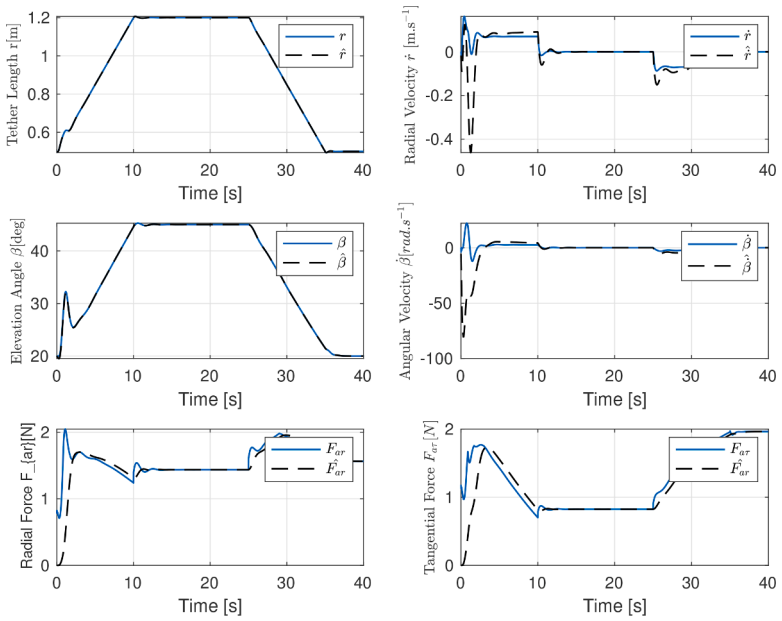

Fig. 5. The estimated state variables by the EKF with Q_1 and R_1 defined in (32) and wind velocity $v_w = 6$ m/s. Solid blue lines show the actual state variable while the dashed black lines correspond to the estimated ones. (For interpretation of the references to colour in this figure legend, the reader is referred to the web version of this article.).

aerodynamic forces.

5.2. Simulation results: estimating both state vector and aerodynamic forces

Notice that, in this simulation case study, the dry friction and the force due to actuator modeling errors are considered only for small wind speed where they are not negligible in front of aerodynamic forces. On the other hand, in this simulation framework, the assumed unknown forces (lift and drag forces) are generated from the formulas (11), (15) and (16).

5.2.1. Discussion on the tuning matrices

It is well known that the performance of an EKF depends mainly on the weighting matrices R and Q. In this study, the used sensors are accurate then the eigenvalues of R should be sufficiently lower than those of Q. On the other side, thanks to the measurements, the length of the tether r and the elevation angle β can be considered accurate in the augmented model (19). Therefore, these state variables should be less weighted compared to the other state variables. Furthermore, since the dynamics of the additive forces are really unknown, the eigenvalues of the matrix Q that correspond to these state variables should be bigger than the others. To illustrate the tuning method, let us consider two tuning examples. In the first one, all the state variables and measurements are identically weighted. That is, the weighting matrices are given

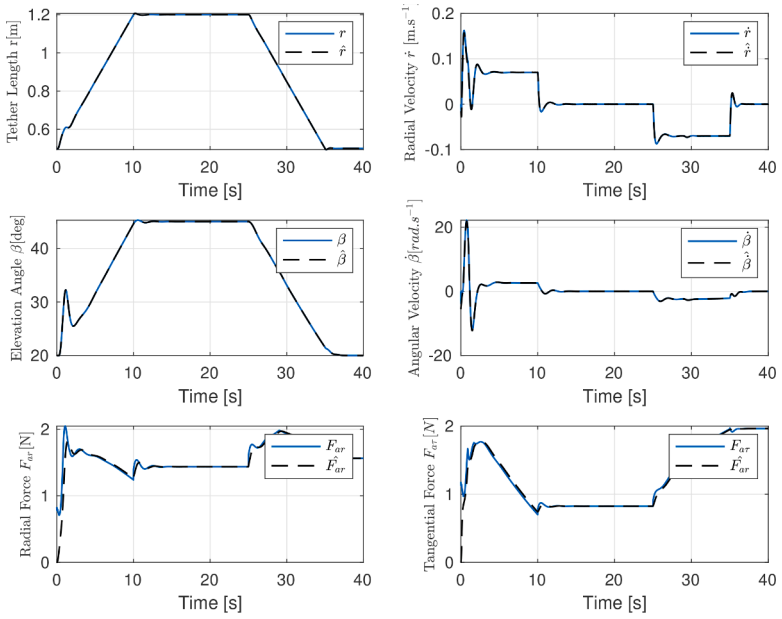

Fig. 6. The estimated state variables with Q_2 and R_2 and wind velocity $v_w = 6$ m/s. Solid blue lines show the actual state variable while the dashed black lines correspond to the estimated ones. (For interpretation of the references to colour in this figure legend, the reader is referred to the web version of this article.).

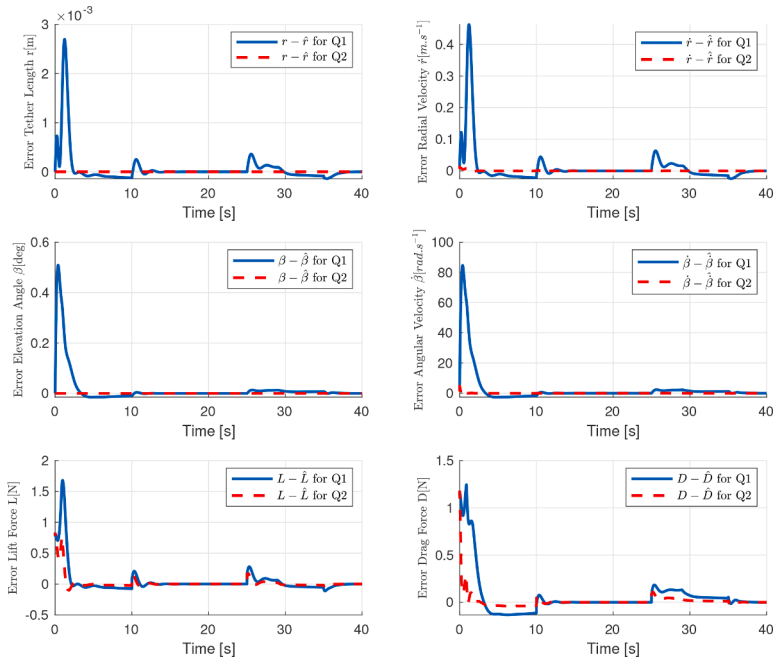

Fig. 7. Comparison of the errors of estimation (calculated separately at each time instant). Solid blue lines show the errors with Q_1 and R_1 while the dashed red lines correspond to Q_2 and R_2. (For interpretation of the references to colour in this figure legend, the reader is referred to the web version of this article.).

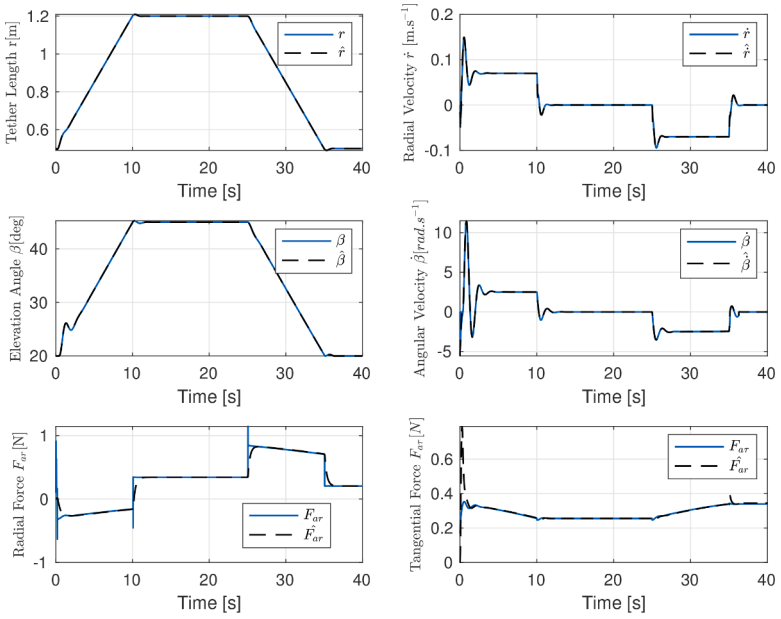

Fig. 8. The estimated state variables compared to those generated by the model, with assumed wind velocity $v_w = 0$ m/s.

by,

$$Q_1 = \begin{bmatrix} 1 & 0 & 0 & 0 & 0 & 0 \\ 0 & 1 & 0 & 0 & 0 & 0 \\ 0 & 0 & 1 & 0 & 0 & 0 \\ 0 & 0 & 0 & 1 & 0 & 0 \\ 0 & 0 & 0 & 0 & 1 & 0 \\ 0 & 0 & 0 & 0 & 0 & 1 \end{bmatrix}, \; R_1 = \begin{bmatrix} 1 & 0 \\ 0 & 1 \end{bmatrix} \tag{32}$$

For the second example, the choice of these matrices is based on the above introduced tuning considerations. That is,

$$Q_2 = \begin{bmatrix} 1^{-10} & 0 & 0 & 0 & 0 & 0 \\ 0 & 5 & 0 & 0 & 0 & 0 \\ 0 & 0 & 1^{-10} & 0 & 0 & 0 \\ 0 & 0 & 0 & 5 & 0 & 0 \\ 0 & 0 & 0 & 0 & 20 & 0 \\ 0 & 0 & 0 & 0 & 0 & 20 \end{bmatrix}, \; R_2 = \begin{bmatrix} 1^{-10} & 0 \\ 0 & 1^{-10} \end{bmatrix} \tag{33}$$

The simulation results with the first tuning Q_1 and R_1 are plotted in Fig. 5, while those of the second tuning Q_2 and R_2 are illustrated in Fig. 6. The estimation errors for both tuning cases are presented in Fig. 7.

As shown in Figs. 5–7, the weighting matrices Q_2 and R_2 provide better results in terms of convergence rate and precision than those generated by the weighting matrices Q_1 and R_1. The obtained simulation

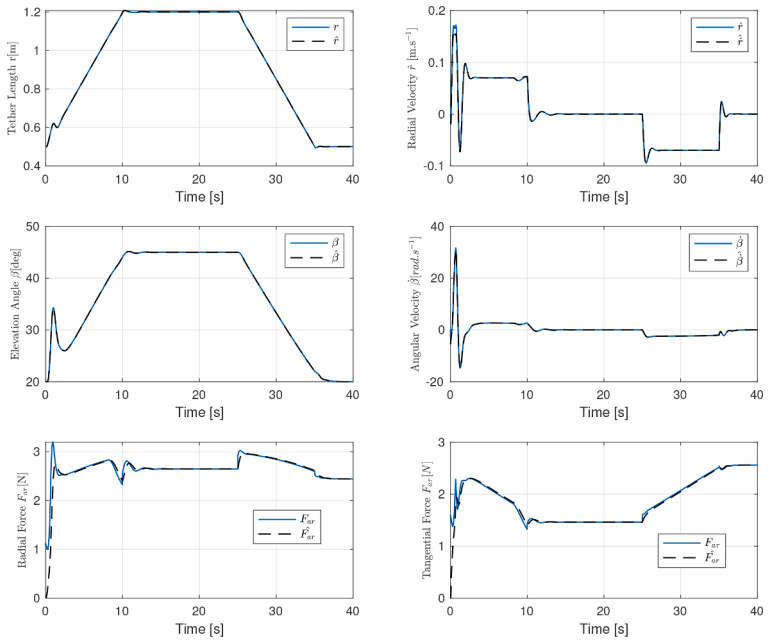

Fig. 9. The estimated state variables compared to those generated by the model, with assumed wind velocity $v_w = 7$ m/s.

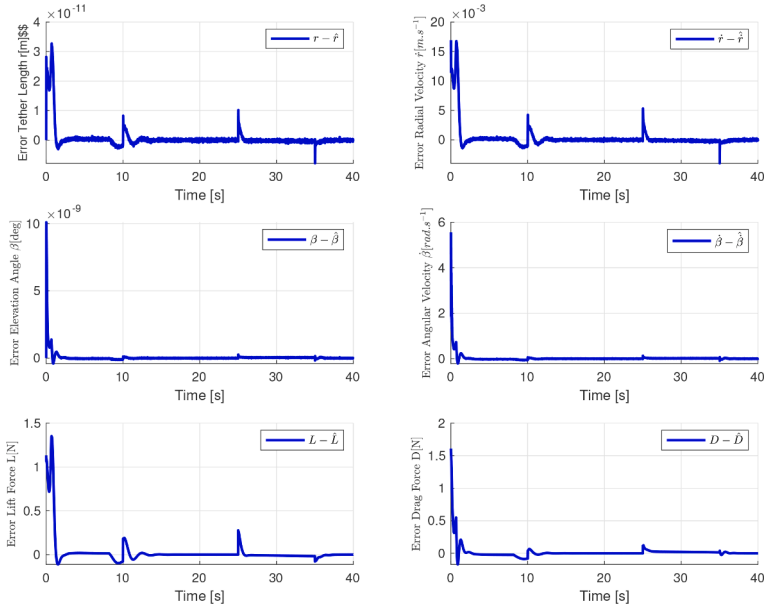

Fig. 10. The error of estimation for the state variables, with assumed wind velocity $v_w = 7$ m/s.

results permit to validate the proposed EKF and the employed tuning method for the weighting matrices. Thus, in what follows, the proposed EKF is applied with the weighting matrices Q_2 and R_2 and its initial state vector is set at:

$$z_0 = (0.5, 0, 0.35, 0, 0, 0)^T \tag{34}$$

This implies that the initial estimates of C_L and C_D are $\widehat{C}_L = 0$ and $\widehat{C}_D = 0$.

5.2.2. *Estimating $F_{a,r}$ and $F_{a,\tau}$ for $v_w = 0$ m/s*

It is worth pointing out that in the case of no wind, $v_w = 0$ m/s, the aerodynamic forces are close to 0 N and the estimated radial and tangential forces correspond to the other forces which are not taken into account in the controller design stage: For instance the dry friction, the forces due to actuators modeling errors, etc. Fig. 8 shows the simulation results obtained in the case of no wind. Note that, the take-off and landing scenario is similar as mentioned above.

As illustrated in Fig. 8, the estimated radial force $\widehat{F}_{a_r}$ plotted in dashed black line converge to the actual one F_{a_r} depicted in solid blue line. Note that this force is composed of the dry friction plus an additive force due to actuator modeling errors as mentioned in Remark 1. As observed, the dry friction is well related to the sign of the reel-in and reel-out speed $\dot{r}$. On the other hand, the estimated tangential force $\widehat{F}_{a_\tau}$ depicted in solid black blue line is mainly formed by the force induced by the actuator modeling errors, which is illustrated in solid blue line.

5.2.3. *Estimating $F_{a,r}$ and $F_{a,\tau}$ for $v_w = 7$ m/s*

For this value of wind speed the magnitude of the aerodynamic

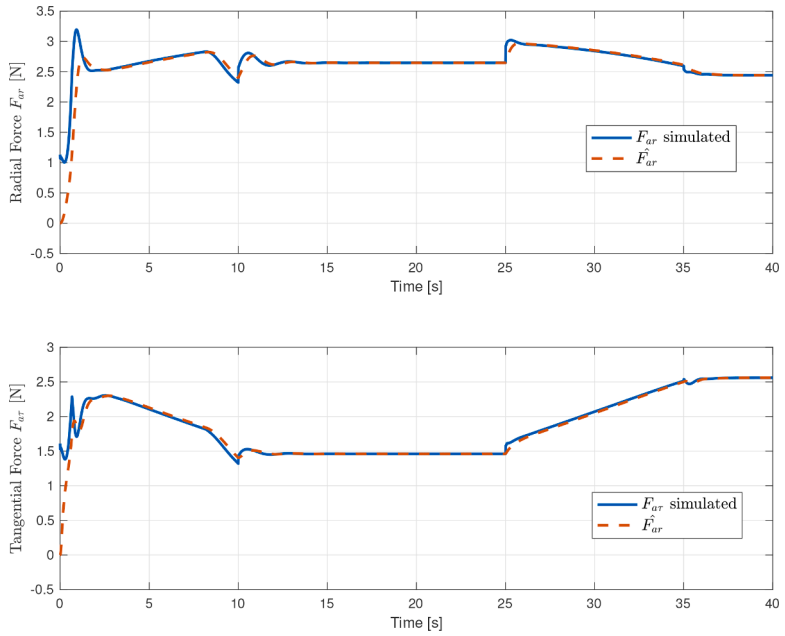

Fig. 11. The estimated aerodynamic forces compared to the assumed actual ones, for $v_w = 7$ m/s.

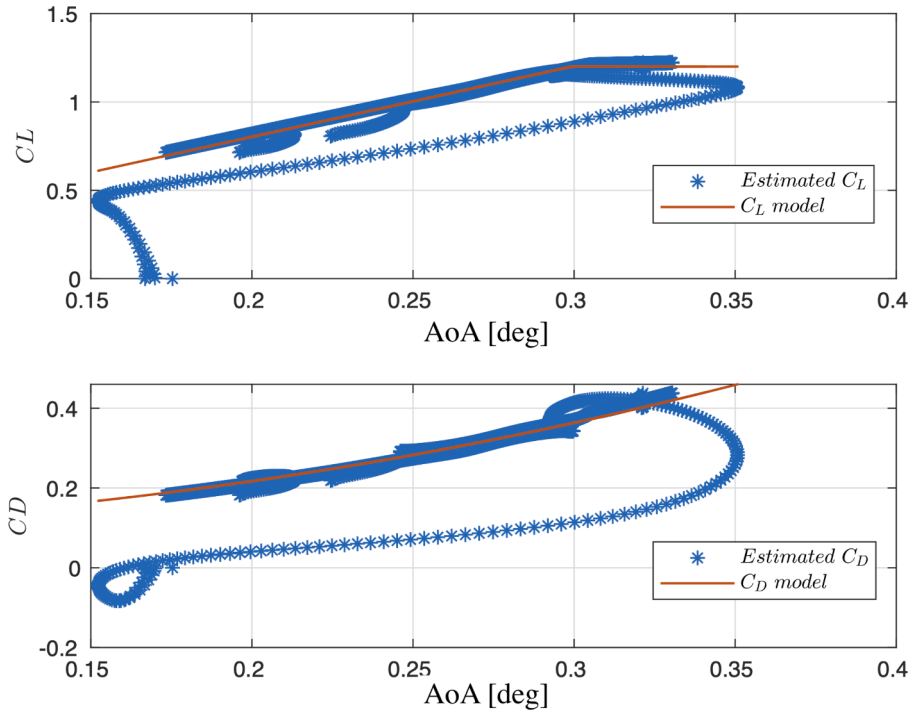

Fig. 12. Estimated versus reference of the aerodynamic coefficients C_L and C_D for $v_w = 6$ m/s.

forces is predominant compared to the magnitude of the dry friction and the magnitude of the force due to actuator modeling errors. Thus they are neglected in this simulation test. The estimated state variables are presented in Fig. 9 together with the assumed actual variables generated by the considered model. As shown by the curves in this figure, the applied EFK has succeeded to provide good estimation results in terms of the accuracy of the estimated augmented state vector and the rapidity of the estimation error convergence.

Moreover, to show clearly the performance (convergence rate and accuracy) of the EKF the time evolution of the estimation errors are plotted in Fig. 10. This figure shows that the initial estimation errors converge rapidly towards weak steady state values. Same remarks and conclusions can be done on the estimated aerodynamic forces plotted in Fig. 11.

5.2.4. *Estimating the aerodynamic coefficients C_L and C_D*

The estimated aerodynamics forces allow one also to deduce a model for the aerodynamic coefficients C_L and C_D by applying relationships (9) and (15). Fig. 12 presents the evolution of the estimated coefficients C_L and C_D computed from the estimated data and those given by model (16) over the observed interval of the variations of angle of attack $AoA = [0.15, 0.35]$.

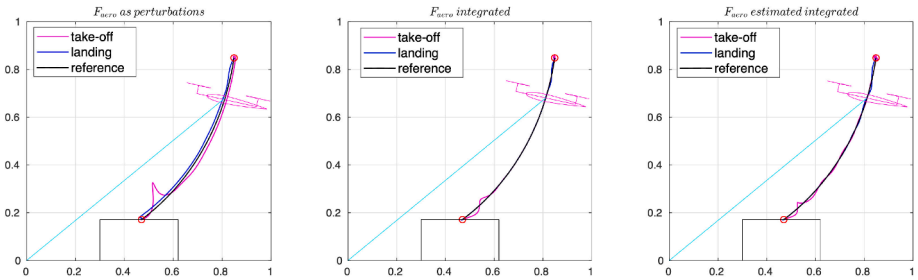

Fig. 13. Flight trajectories of the AWE system driven by different control strategies for $v_w = 6$ m/s.

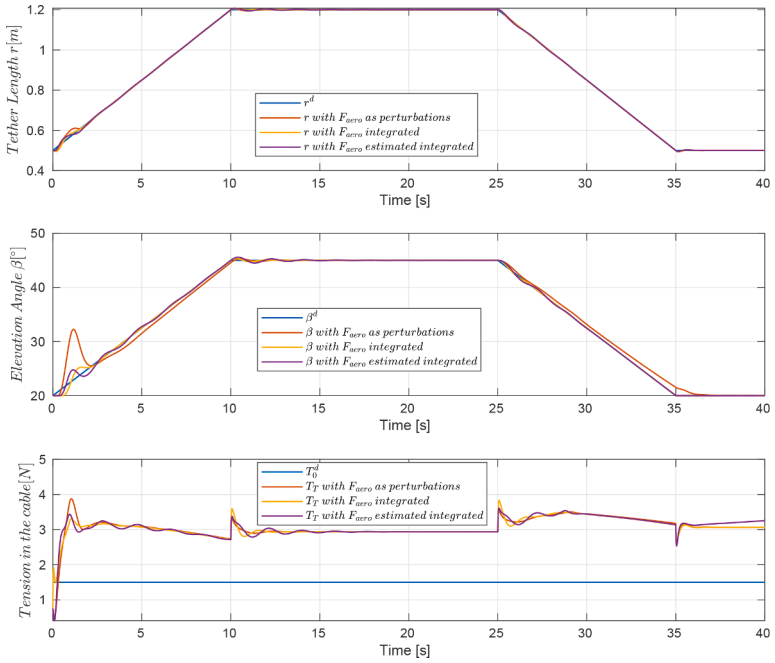

Fig. 14. The time evolution of r, β and T_T for $v_w = 6$ m/s.

As shown in Fig. 12, the estimated values of C_L and C_D converge rapidly towards those provided by the model. By estimating these parameters for the whole range of possible angle of attack, a good aerodynamic model of the system can be identified. However, to be able to do these estimations, a measure of the wind speed is required.

Remark 3. It is worth pointing out that, thanks to the proposed EKF, the wind velocity can be estimated if an accurate model of the aerodynamic coefficients is available.

5.3. Integrating the aerodynamic forces in the control law

In this Section, we propose to integrate the estimated aerodynamic forces in the design of the output-feedback linearization control law introduced in Schanen et al. (2021). That is, we have applied the control law defined by (29)-(31) and implemented as shown in the second closed-loop of Fig. 4. This allows one to better deal with the system uncertainties and so to enhance its robustness. Note that, in Schanen et al. (2021) the unknown aerodynamic forces are considered as external disturbances and integral actions are used to attenuate their effect on the desired behavior of the system. The simulation results of the controlled system are shown in Figs. 13 and 14. Three control configurations are considered in these figures. The red lines correspond to the control law presented in Schanen et al. (2021) where the aerodynamic forces are considered as disturbances. The yellow lines show the results of the ideal case where the aerodynamic forces are assumed perfectly known and integrated directly in the control step. Finally, the purple lines correspond to the case where the estimated aerodynamic forces are used in the design step of the controller. As expected, the knowledge of these forces allows one to obtain better results in terms of the tracking performance. As illustrated in Fig. 13, thanks to the use of the EKF, the static deviation of the AWE system from its set-point trajectory is considerably reduced. Fig. 14 shows the time evolution of the three controlled variables: two state variables (the tether's length r and the elevation angle β) and the tension in the tether T_T for the three considered control configurations. Notice that, in this figure r^d, β^d and T_0^d correspond to the desired target trajectories (set-points). Based on the simulation results, it is clear that the main improvement is about the elevation angle, which has less steady-state error and a smaller overshoot at the beginning of the take-off phase.

To sum up, the different simulation results show that by considering the aerodynamic forces in the control design step, the performance of the closed-loop system is improved. Moreover, the proposed EKF succeeds to provide accurate estimates of the state vector of the system and the unknown forces acting on it.

5.4. Experimental results

In this Section, the proposed Extended Kalman filter is applied offline on the experimental data extracted from the experiments carried out in Schanen et al. (2021) for no wind speed (i.e $v_w = 0$ m/s). It is worth pointing out that our experimental facility does not include an adequate

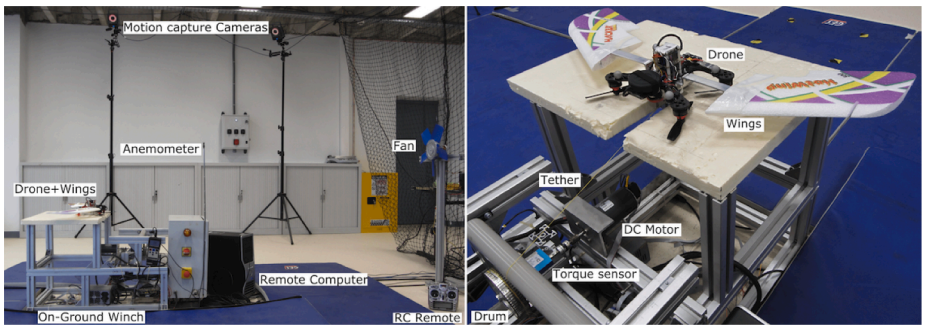

Fig. 15. The different components of the benchmark.

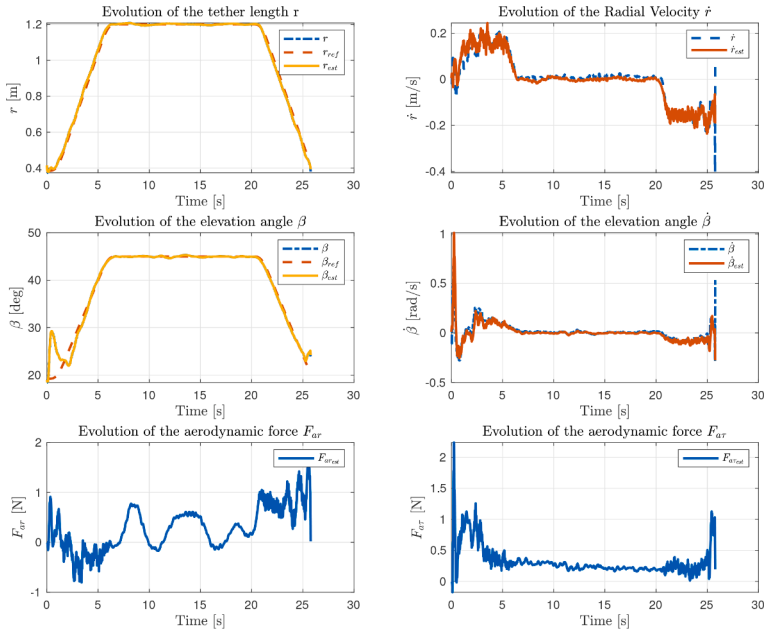

Fig. 16. Estimation of the actual state variable for $v_w = 0$ m/s.

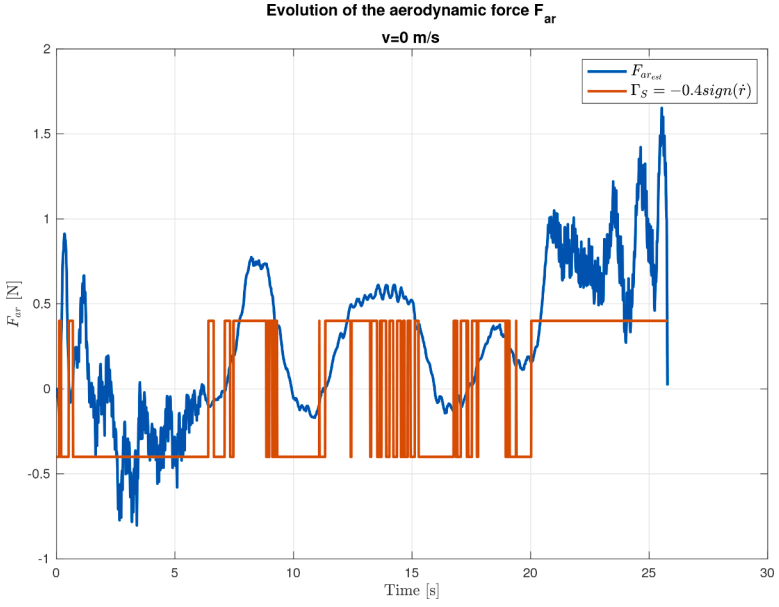

Fig. 17. Estimated radial force compared with a model of static friction in the ground station.

wind tunnel that could produce significant and relatively stable lift and drag force on the system.

The experimental benchmark is composed of wings attached to a drone and linked together to an on-ground winch with a tether. A motion capture system tracks the drone position and sends it to an on-ground computer that controls the winch and the drone. Fig. 15 shows the global architecture of the system. It is worth pointing out that detailed description of all the components of this experimental setup is available in Schanen et al. (2021).

In order to better adapt to the uncertainties of the experimental framework and to converge faster towards the actual values of the unknown forces, the weighting matrices of EKF were adjusted as follows:

$$Q_3 = \begin{bmatrix} 1^{-3} & 0 & 0 & 0 & 0 & 0 \\ 0 & 1 & 0 & 0 & 0 & 0 \\ 0 & 0 & 1^{-3} & 0 & 0 & 0 \\ 0 & 0 & 0 & 1 & 0 & 0 \\ 0 & 0 & 0 & 0 & 200 & 0 \\ 0 & 0 & 0 & 0 & 0 & 200 \end{bmatrix}, \; R_3 = \begin{bmatrix} 1^{-10} & 0 \\ 0 & 1^{-10} \end{bmatrix} \tag{35}$$

Note that, this experiment was performed with the same scenario exhibited in Subsection 5.1. In Fig. 16 the estimated variables provided by the EKF and the measured ones are compared in the case of $v_w = 0$ m/s.

As mentioned previously, since there is no wind, the estimated forces are not the aerodynamic ones, but reflects other forces that are not included in the prediction model used in the EKF algorithm. In particular, the estimated radial force is very close to the behavior of a dry friction as it can be seen in Fig. 17. Fig. 16 also illustrates that the estimated variables $\hat{r}$, $\dot{\hat{r}}$, $\hat{\beta}$ and $\dot{\hat{\beta}}$ are very close to the measured ones, which confirms further the good performance of the proposed EKF. On the other hand, the tangential part of the estimated force is highly correlated (cross correlation = 0.833) to the tangential projection of the drone thrust T_D. We can conclude that the EKF gives a good estimation of the difference between the desired drone thrust and the actual one.

6. Conclusion

A dynamical estimation method based on the theory of Extended Kalman Filter is proposed in this work for an AWE system during its take-off and landing phases. This method allows one to estimate accurately the state vector of the system, the unknown forces that act on it and its aerodynamic coefficients. Moreover, if a reliable model of these coefficients is available the proposed algorithm can estimate also the wind velocity. The performance of this estimation algorithm is validated in both simulation and experimental frameworks. It is worth pointing out that the assumption that the tether forms a straight line is valid for small length, where drag and weight of the cable are negligible w.r.t tether tension, and tether elasticity is low. In future work, a more accurate model of tether will be used in order to get accurate results also for higher length of cables.

On the other hand, we have shown that by integrating the estimation results in the control design step, the performance of the nonlinear controller introduced in Schanen et al. (2021) is improved and its robustness with respect to uncertainties is enhanced. Based on these results, several orientations to pursue this work in future are possible. For instance, it could be possible to use the estimated aerodynamic forces as auxiliary actuators to improve the performance of the proposed control laws and thus dealing with higher wind velocities.

CRediT authorship contribution statement

Nacim Meslem: Conceptualization, Methodology, Validation, Writing – original draft. **Jonathan Dumon:** Methodology, Validation, Software, Resources. **Ahmad Hably:** Supervision, Validation, Writing – original draft. **Asmae El Ayachi:** Software, Writing – original draft. **Audrey Schanen:** Methodology, Software.

Declaration of Competing Interest

The authors declare that they have no known competing financial interests or personal relationships that could have appeared to influence the work reported in this paper.

Acknowledgment

The equipment used in the paper was partially funded by Equipex Robotex (ANR-10-EQPX-44-01).

References

Ahmed, M., Hably, A., & Bacha, S. (2012). High altitude wind power systems: A survey on flexible power kites. *Proceedings of the xxth international conference on electrical machines* (pp. 2085–2091). IEEE.

Airborne wind energy. In Ahrens, U., Diehl, M., & Schmehl, R. (Eds.), *Green Energy and Technology*, (2013). Springer.

Archer, C., & Caldeira, K. (2009). Global assessment of high-altitude wind power. *Energies, 2*, 307–319.

Canale, M., Fagiano, L., & Milanese, M. (2010). High altitude wind energy generation using controlled power kites. *IEEE Transactions on Control Systems Technology, 18(2)*, 279–293.

Cherubini, A., Papini, A., Vertechy, R., & Fontana, M. (2015). Airborne wind energy systems: A review of the technologies. *Renewable and Sustainable Energy Reviews, 51*, 1461–1476.

Daum, F. E. (2015). *Extended Kalman filters*. In J. Baillieul, & T. Samad (Eds.) (pp. 411–413)). London: Springer London.

Fliess, M., Lévine, J., Martin, P., & Rouchon, P. (1995). Flatness and defect of non-linear systems: introductory theory and examples. *International Journal of Control, 61*(6), 1327–1361.

Hably, A., Dumon, J., Smith, G., & Bellemain, P. (2018a). Control of a magnus effect-based airborne wind energy system. *Airborne wind energy* (pp. 277–301). Springer.

Hably, A., Dumon, J., Smith, G., & Bellemain, P. (2018b). *Control of a magnus effect-based airborne wind energy system*. Singapore: Springer Singapore. https://doi.org/10.1016/j.ifacol.2017.08.2205

Hjukse, O. H. (2011). State estimation and kalman filtering of tethered airfoils: by use of ground based meausrments. Master's thesis.Institutt for teknisk kybernetikk.

Jaulin, L. (2015). *Mobile robotics*. ISTE Ltd 27–37 St George's Road London SW19 4EU United Kingdom: ISTE, ELSEVIER.

Ljung, L. (1979). Asymptotic behavior of the extended Kalman filter as a parameter estimator for linear systems. *IEEE transactions on automatic control, 24*, 36–50.

Lozano, R., Dumon, J., Hably, A., & Alamir, M. (2013). Energy production control of an experimental kite system in presence of wind gusts. *Proceedings of the iEEE/RSJ international conference on intelligent robots and systems* (pp. 2452–2459). IEEE.

Millane, A., Hesse, H., Wood, T. A., & Smith, R. S. (2015). Range-inertial estimation for airborne wind energy. *Proceedings of the 54th IEEE conference on decision and control (cdc)* (pp. 455–460). IEEE.

Ranneberg, M. (2013). Sensor setups for state and wind estimation for airborne wind energy converters. *arXiv preprint arXiv:1309.1029*.

Schanen, A., Dumon, J., Meslem, N., Hably, A., Nègre, A., & Sarazin, A. (2021). Tethered drone-based airborne wind energy system launching and retrieving. *Journal of Guidance, Control, and Dynamics, 44*(11), 2284–2293.

Schmehl, R. (2018). *Airborne wind energy: Advances in technology development and research*. Springer.

Schmidt, E., De Lellis, M., Saraiva, R., & Trofino, A. (2017). State estimation of a tethered airfoil for monitoring, control and optimization. *IFAC-PapersOnLine, 50*(1), 13246–13251.

Simon, D. (2010). Kalman filtering with state constraints: A survey of linear and nonlinear algorithms. *IET Control Theory & Applications, 4*(8), 1303–1318.

Williams, P., Lansdorp, B., & Ockels, W. (2008). Nonlinear control and estimation of a tethered kite in changing wind conditions. *Journal of guidance, control, and dynamics, 31*(3), 793–799.

Zgraggen, A. U., Fagiano, L., & Morari, M. (2014). Real-time optimization and adaptation of the crosswind flight of tethered wings for airborne wind energy. *IEEE Transactions on Control Systems Technology, 23*(2), 434–448.